IEEE Photonics Journal
An IEEE Photonics Society Publication

Open Access

Deflection Monitoring Method Using Fiber Bragg Gratings Applied to Tracking Particle Detectors

Volume 6, Number 6, December 2014

Agostino Iadicicco
Massimo Della Pietra
Mariagrazia Alviggi
Vincenzo Canale
Stefania Campopiano

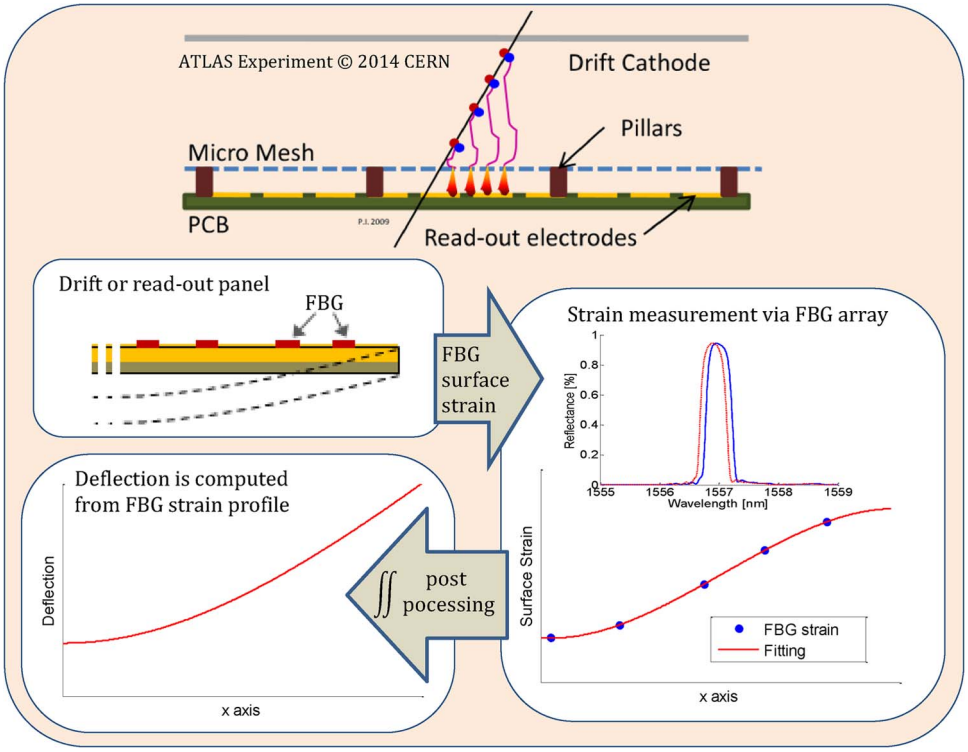

DOI: 10.1109/JPHOT.2014.2352639
1943-0655 © 2014 IEEE

Deflection Monitoring Method Using Fiber Bragg Gratings Applied to Tracking Particle Detectors

Agostino Iadicicco,[1] Massimo Della Pietra,[1,2] Mariagrazia Alviggi,[2,3] Vincenzo Canale,[2,3] and Stefania Campopiano[1]

[1]Engineering Department, University of Naples "Parthenope", 80143 Napoli, Italy
[2]Istituto Nazionale di Fisica Nucleare, Sezione di Napoli, 80126 Napoli, Italy
[3]Physics Department, University of Naples Federico II, 80126 Napoli, Italy

DOI: 10.1109/JPHOT.2014.2352639
1943-0655 © 2014 IEEE. Translations and content mining are permitted for academic research only. Personal use is also permitted, but republication/redistribution requires IEEE permission. See http://www.ieee.org/publications_standards/publications/rights/index.html for more information.

Manuscript received June 11, 2014; revised August 4, 2014; accepted August 7, 2014. Date of publication August 28, 2014; date of current version December 18, 2014. Corresponding author: A. Iadicicco (e-mail: iadicicco@uniparthenope.it).

Abstract: This paper proposes the use of fiber Bragg gratings (FBGs) for the deflection monitoring of a micromegas (MM) tracking particle detector to be installed at the European Organization for Nuclear Research during a major upgrade of the experiment ATLAS within 2018. MM detectors are designed to reach high spatial and time resolution, even if the design is not yet finalized. One mandatory issue for the MM detector is a precise monitoring of the deflection of the drift and read-out electrodes and/or of the panel hosting the electrodes. To this aim, FBG strain sensors are proposed and experimentally investigated as a sensing solution to monitor the strain state of the detector support panel hosting the drift and read-out electrodes. Finally, simple postprocessing analysis based on classical beam theory considering a rigid body permits calculating the panel deflection. Preliminary experimental results on first prototypes of small and large detector panels are presented and discussed.

Index Terms: Fiber Bragg sensors, deflection monitoring, high-energy physics, tracking detectors.

1. Introduction

The Large Hadron Collider (LHC) [1] at the European Organization for Nuclear Research (CERN) has been designed to produce proton-proton collisions at the energy of 14 TeV to study the elementary constituents of the matter and their interactions. And, four experiments have been built [1] (ATLAS, CMS, LHCb, ALICE) around the interaction points of the accelerator. A measurement of the momentum of the charged particles produced in the collisions is obtained by measuring the curvature of their tracks in a magnetic field. To achieve a resolution of about 10% for particles with 1 TeV/c momentum it is necessary to measure the charged particles track with a space resolution of the order of 100 μm. So far, several detectors have been adopted to this goal and new ones have been designed to improve the performance.

Our attention is focused on micromegas [2] [an abbreviation for "micro mesh gaseous structure" (MM)], that is a gaseous particle detector. MM will be installed as a tracking detector in the ATLAS experiment [3] at LHC by the end of 2018, during a major upgrade of the experiment. The design of this upgrade has been done but not yet finalized. MM detectors consist of a planar

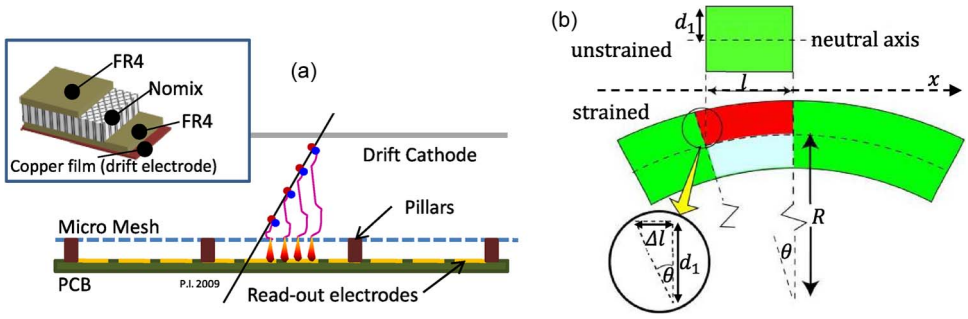

Fig. 1. (a) Micromegas detector and its working principle (ATLAS Experiment 2014 CERN). (Insert) Schematic view of the drift panel (support panel with drift electrode). (b) Schematic view of a beam subjected to a bending moment.

electrode (drift electrode), a gas gap of a few millimeters thickness and a thin metallic mesh at typically 100–150 μm distance from the readout electrode [4], as schematically plotted in Fig. 1(a). Briefly, charged particles traversing the drift space ionize the gas, the electrons liberated by the ionization process drift towards the mesh following an electric field of about few hundred Volt/cm. Beyond the mesh, a stronger electric field creates an electron avalanche in the thin amplification region, immediately above the readout electrodes; this avalanche gives a current pulse on the readout electrodes, that is segmented in strips, thus allowing a space reconstruction of incident particle track. The MM is designed to achieve space and time resolution of about 100 μm and 5 ns, respectively. To achieve this performance the geometry of any tracking detector has to be known with a precision of few tens of μm. The relative position of each detector with respect to a reference system can be measured through optical sensor elements (CCDs, lenses, light sources), but any deflection of drift and read-out electrodes has to be monitored as well.

In current MM design, drift and read-out electrodes are made with uniform and patterned copper films (about 35 nm thick), respectively, deposited on two support panels. Each panel is formed by an honeycomb core with two skins of a composite material made of woven fiberglass cloth with an epoxy resin binder (FR4). The insert in Fig. 1 schematically plots the multilayer structure of the drift panel (support panel with drift electrode).

Thus, a sensing system capable to detect any curvature/strain/deflection of the tracking detector with a resolution of few tens of μm is desirable. However any sensor to be introduced in the detector volume should ideally comply with many requirements in terms of radiation hardness, resistance, insensitivity to magnetic field, small dimensions and low mass, and minimal need of services. On this line of argument fiber optic sensors (FOSs) seem to have the potential to provide a perfectly suited solution to realize high sensitive sensors to be integrated with [5], [6]. Indeed, the fiber itself can tolerate very high levels of radiations [7]–[9]. In particular, among FOSs, fiber Bragg gratings (FBGs) and long period gratings (LPGs) in conventional and unconventional fibers have gained great popularity in sensing applications for their intrinsic capability to sense physical (strain and temperature) and chemical (especially for LPGs) parameters with wavelength-encoded information [10]–[16] and for their advantageous features like wavelength-encoded information, reduction of cabling complexity, availability and cost of the device. However in the most sensing applications where it is requested to have a multipoint measurements of physical parameters such as strain and temperature or temperature compensated strain, FBG sensors are preferred [10]–[12] for their additional advantageous characteristics like high multiplexing capability, linear output, and assessment of reliable interrogation units.

According to this, in this work, for the first time to our best knowledge, we propose the use of FBG strain sensors as suitable sensing solution for the deflection monitoring of the tracking particle detector and in particular of the support panels hosting the drift and read-out electrodes. The basic idea is to calculate the panel deflection from the surface strain measured by means of an appropriate FBG array [17], [18]. It is worth highlighting that even if we report an experimental feasibility analysis without taking into consideration the environmental condition in terms

of ionizing radiations present at CERN, the FBG sensors radiation hardness capability has been well investigated [7], [9]. In particular it was demonstrated that no significant variations in the Bragg wavelength occurred after the ionizing radiations and only a small shift of a few tens of picometers was observed [9] making such technology appropriate to operate at CERN condition.

The paper is organized as follow. In Section 2, the methodology will be briefly illustrated. In Section 3, the experimental results on a miniaturized support panel will be shown. In Section 4, preliminary results on a full size panel will be reported. The achieved results of the proposed methodology let us believe that it will be take into consideration for the final update of ATLAS experiment. The complete investigation on a full size panel in terms of deflection monitoring during several steps of the first detector prototype fabrication is currently in progress.

2. Methodology

The basic idea is to use the FBGs as strain sensors in order to detect the deflection of a generic beam. It is well known that an FBG consists of a periodic modulation of the core refractive index along a segment of an optical fiber (long from few mm to 10 mm) [10]–[12]. The FBG is specified by the Bragg wavelength, which is given by $\lambda_B = 2n_{\text{eff}}\Lambda$, where n_{eff} is the core mode effective refractive index and Λ is the grating period. The shift in the Bragg wavelength due to strain ε and temperature ΔT changes is given by [10]:

$$\frac{\Delta\lambda_B}{\lambda_B} = S_\varepsilon \varepsilon + S_T \Delta T \tag{1}$$

where λ_B is the original Bragg wavelength, $\Delta\lambda_B$ is the variation in Bragg wavelength due to applied strain ε and temperature variation ΔT, and S_ε and S_T are the sensitivity coefficients to strain and temperature, respectively. According to (1), FBG sensors permit accurate measurement of the strain profile of the support panel surfaces where some FBGs are bonded to (or embedded in) whereas thermal effects can be properly compensated by using an additional FBG [11].

However to meet our aim it is worth noting that the deflection can be evaluated by classical beam theory with small deformation assumption. In particular, a second derivative relationship exists between the displacement orthogonal to the surface and the strain component parallel to it, as extensively reported elsewhere [19]. Briefly here, a schematic view of a solid beam (with which we will schematize the detector panel in our study case) bent to a (uniform) radius of curvature, R, is plotted in Fig. 1(b). Indeed, here for sake of simplicity, we schematize a 1-D beam (along x axis) while the same approach could be extended to xy plane. Considering a section of length l (unstrained) and the same after bending, the bending angle is $\theta = l/R$. The bending induces compressive strain on the "inside" surface of the beam (colored light blue) and tensile strain on the "outside" surface (colored red). θ is also given by length change Δl divided by distance from neutral axis d_1. The surface strain component along x, $\varepsilon(x) = \Delta l/l$, is thus given by the ratio d_1/R. Since the curvature $C = 1/R$ is defined as second derivate of the displacement profile $\omega(x)$ [19], [20], the strain component along x, can be written as:

$$\varepsilon_x(x) = -d_1 \frac{\partial^2 \omega(x)}{\partial x^2}. \tag{2}$$

Following our idea, the whole surface of the support panels can be sensitized by using FBGs bonded to it in order to measure the surface strain profile. Thus the strain curve along x direction can be fitted with a polynomial $P_n(x)$ of degree n in order to achieve a continuous function for the strain. To compute the panel displacement we can integrate (2) as a function of x:

$$\omega(x) = -\frac{1}{d_1}\int\left(\int P_n(x)dx\right)dx = P_{n+2}(x) + C_1 x + C_0 \tag{3}$$

The terms C_1 and C_0 are two constants that can be calculated using appropriate boundary conditions including considerations about eventually structural symmetry, eventually known

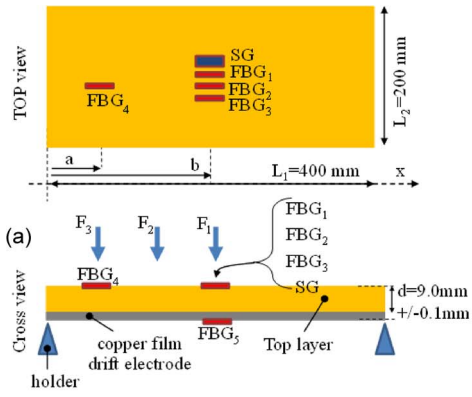

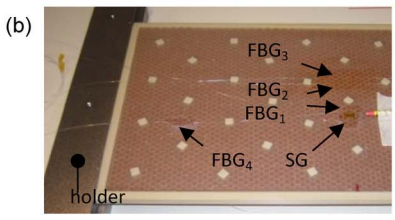

(c)

Grating	Wavelength	Coating	Adhesive	Position
FBG_1	1557.0 nm	bare	Cyanoacrylate	Centre/Top
FBG_2	1541.4 nm	bare	Araldite	Centre/Top
FBG_3	1533.4 nm	polyamide	Araldite	Centre/Top
FBG_4	1549.1 nm	bare	Cyanoacrylate	Lateral/Top
FBG_5	1565.3 nm	polyamide	Cyanoacrylate	Centre/Back
FBG_T	1552.9 nm	--	--	Free

Fig. 2. (a) Schematic cross and top view of the miniaturized panel. (b) Picture of the panel with FBGs and SG sensors. (c) FBG characteristics.

displacement in specific x point, the continuity of $\omega(x)$ and/or of $d\omega(x)/dx$. Actually, C_0 acts as offset, and thus, it has a poor meaning in applications where it is necessary to detect the deflection changes.

The simplicity of this approach permits to apply it to a generic solid beam. The most critical issue in the proposed approach is the right selection of the FBG number. It should be large enough to accurately measure the strain profile and the smallest possible to decrease the cost and complexity. About detectors support panels, currently, FEM analysis is under development in order to determine the optimized number and position of FBG strain sensors to be integrated with panel.

In the following section we will show preliminary experimental tests aimed to investigate the capability to measure the surface strain and thus the deflection according with (3) of first miniaturized and then full size prototypes of detectors support panel.

3. Experimental Results: Small Support Panel

Here we focus the attention on a miniaturized preliminary support panel. Experimental results aimed to validate the proposed approach when the displacement of the support panel is induced by applying concentrate weight in different positions are reported and discussed. The miniature panel sizes are of $L_2 = 200$ mm and $L_1 = 400$ mm whereas the thickness of $d = 19.0$ mm $+/-0.1$ mm and the composition structure is the same of the final drift/read-out panel. Here, a honeycomb flame-resistant meta-aramid material (NOMEX) core was used. In the following, it is simply schematized as a two-layer panel involving a composite top layer and a copper film, as plotted in Fig. 1(a). A set of five commercial FBGs with different Bragg wavelength are properly bonded to the surface of the miniaturized panel with different adhesives and positions. All gratings were released in standard SMF-28e fiber. Bare FBGs and FBGs with protective polyamide coating have been selected and bonded with the aim to compare them, in terms of $\Delta\lambda_B$, since the former is easy to fix ensuring maximum strain transfer whereas the last one is more robust in handle operations. Different adhesives such as Araldite 2011 and a Cyanoacrylate-base adhesive have been used in order to validate the strain transfer capability of the former one that is already certificate for the operation at CERN. About sensor position, FBG_1, FBG_2, and FBG_3, with different coatings are fixed (very close each other) in the center of the top side of the panel (FR4 side) with different adhesives. The FBG_4 is fixed at a distance of $a = 6.2$ cm from left side and the FBG_5 is fixed on the back side (copper film) in specular position with respect to FBG_1. Finally the FBG_T consists in a commercial FBG with ceramic package and known thermal characteristic useful to compensate the thermal effect and thus it was not glued. Moreover the responses of FBGs are compared with a conventional resistive strain gauges (SG) fixed close to FBG_1. A summary of FBGs characteristics is reported Fig. 2(c), while a picture of the FR4 side of the miniaturized panel is shown in Fig. 2(b).

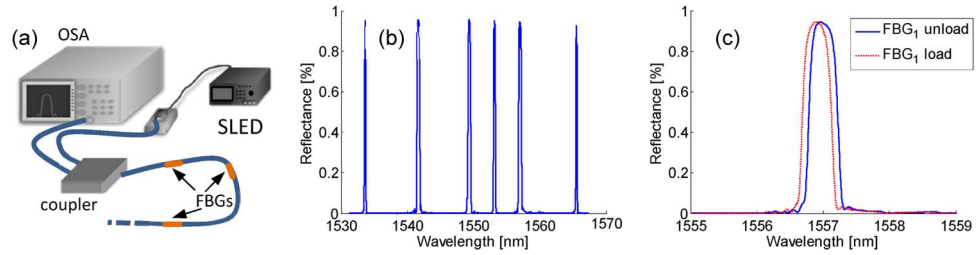

Fig. 3. (a) Scheme of the optoelectronic setup; (b) reflectance spectrum of all gratings in the unload state; and (c) spectra of FBG_1 sensor in load and unload states.

Reflectance spectra were carried out by means of a optoelectronic setup involving a 3 dB coupler placed between a broadband light source (Superluminescent LED) and the fiber with FBGs serially connected where one return end is sent to optical spectrum analyzer (OSA-Yokogawa AQ6317B), as schematically plotted in Fig. 3(a). The reflectance spectrum of all gratings in the unload state in plotted in Fig. 3(b). SG measurements were carried out by means of an standard Digital Multimeter.

All FBG strain sensors have been previously characterized in terms of their strain and temperature sensitivities exhibiting $S_T = 5.4 \cdot 10^{-6}\ ^{\circ}C^{-1}$ and $S_\varepsilon = 0.815 \cdot 10^{-6}\ \mu\varepsilon^{-1}$, and thus strain measurement with resolution lower than 1 $\mu\varepsilon$ are possible [10], [11]. The Bragg wavelengths are retrieved via centroid analysis of the reflected spectra. During the experiments temperature was kept constant within 0.5 °C. However, the small temperature changes are compensated by using FBG_T.

In order to investigate the sensor response to the panel deflection, the panel itself is positioned on two rigid holders while several masses with weight up to 1432 g (named $W_0 = 0$ g, $W_1 = 269$ g; $W_2 = 537$ g; $W_3 = 800$ g; $W_4 = 1432$ g, respectively) are applied in different points along the panel length (x axis), F_1, F_2, F_3, and F_4. The position F1 is selected as center of the detector support $(b = 20\ cm)$ and thus in correspondence of FBG_1, FBG_2, FBG_3, and SG sensors; F_3 is selected in correspondence of FBG_4 $(a = 6.2\ cm)$; F_2 is about in the center between F_1 and F_3 $(x = (a + b)/2 = 13.1\ cm)$; and F_4 is selected far from F_2 side (for $x = 26$ cm). A comparison of the reflectance spectra of the FBG_1 in case of unload and load (with W_4 weight in the center of the panel) states is plotted in Fig. 3(c) as example of sensor operation; the Bragg wavelength shifts of approximately 100 pm.

In the following we first investigate the effect of a symmetric deformation of the panel by applying several masses on the F1 position and successively investigate the effect of the mass position.

3.1 Symmetric Load

The Fig. 4(a) plots the strain measurements of optical and electrical sensors versus the time (with scan step of 15 seconds) during a stepwise weight increment (load) and decrement (unload), applied on position F_1. From these data some important results can be highlighted. FBG_1, FBG_2, FBG_3, and FBG_4 record a negative strain while FBG_5 records a positive strain. This means that, as expected, the top layer surface is compressed while the opposite surface (bottom copper layer) is stretched. Also, it can be noted that responses of FBG_1, FBG_2, FBG_3, and SG are in perfect agreement (within $+/-1$ $\mu\varepsilon$). This means that bare and polyamide FBGs are both well candidate for our purpose and Araldite 2011 permits a full strain transfer operation. To highlight the capability to measure the strain distribution along the panel, we also compare the responses of the FBG_4 with FBG_1, FBG_2, and FBG_3. FBG_4 retrieves a lower strain (as absolute value) as compared with the FBGs positioned in the center/top of the support panel. The ratio of FBG_4/FBG_i (with $i = 1, 2, 3$) in terms of Bragg wavelength shift is very close to the ratio of their position a/b [see Fig. 1(a)] of 0.31. Furthermore, the absolute value of the strain detected from FBG_1, FBG_2, and FBG_3 is about two times higher than the output of FBG_5, as expected for an

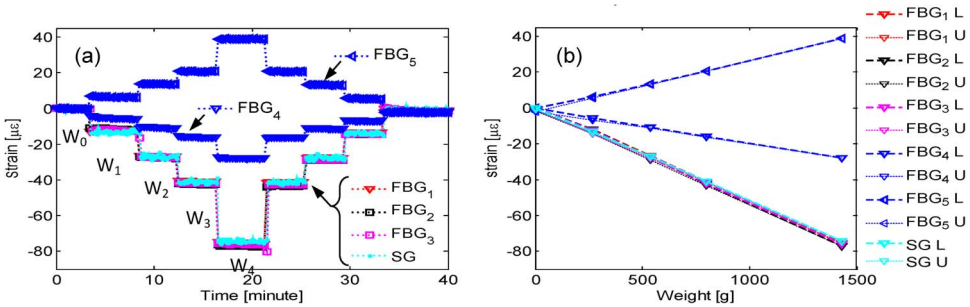

Fig. 4. Strain measurements of the five FBGs and the SG (after thermal compensation). (a) Strain versus time and as function of the applied mass (W_0, W_1, W_2, W_3, and W_4). (b) Strain versus applied mass during load (L) and unload (U) phases.

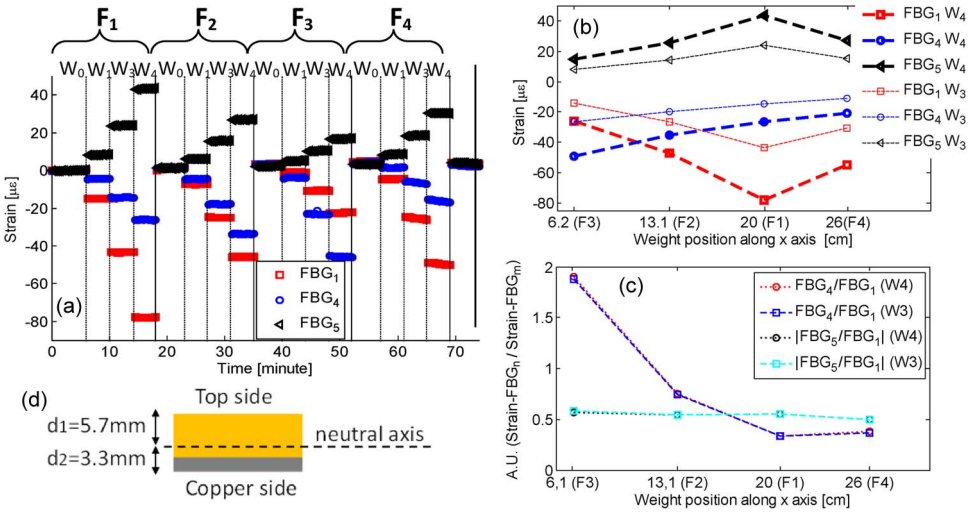

Fig. 5. Strain measurements of the FBG_1, FBG_4, and FBG_5 (after thermal compensation). (a) Strain versus acquisition time and as function of the applied mass (W_0, W_1, W_3, and W_4) and mass position (F_1, F_2, F_3, and F_4). (b) Strain versus weight position along x axis as function of the applied mass. (c) Strain ratio of FBG_4/FBG_1 and FBG_5/FBG_1 (in absolute value) vs weight position along x axis and as function of the applied mass. (d) Neutral axis position.

inhomogeneous panel. Finally, Fig. 4(b) plots the strain versus weights during the load and unload phases. As evident all sensors (FBGs and SG) show a linear response versus the applied weight and a very good agreement between the load and unload phases.

3.2 Asymmetric Load

We also investigate the effect on the measured strain when the applied mass on the top surface moves from the center of the panel towards lateral position. Fig. 5(a) plots the responses of FBG_1, FBG_4, and FBG_5 (for simplicity, FBG_2 and FBG_3 are omitted) versus the time during a stepwise weight increment applied in F1, F2, F3, F4 position, respectively. As the mass moves from the center towards F_2 and then F_3 (close to FBG_4 sensor) the amplitudes of the responses (in absolute value) of FBG_1 and FBG_5 decrease and the output of FBG_4 increases. The FBG_4 reaches its maximum sensitivity when mass is in F_3. Moreover in the position F_4 the strain of FBG_1 and FBG_5 are comparable to the values in position F_2 whereas the output of FBG_4 further decreases. Fig. 5(b) summarize the data by plotting the FBGs responses versus the mass position for different weights (W_3 and W_4).

Fig. 5(c) shows that strain ratio of FBG_4/FBG_1 is not dependent on the applied mass but only on the position of the mass along the panel length. This consideration reveals that the

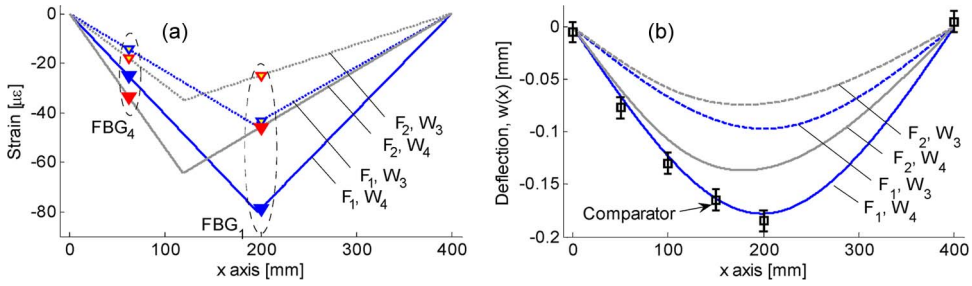

Fig. 6. (a) Strain profile of the miniaturized panel vs x axis as function of weight and its position. (b) Deflection calculated from data of (a).

ratio of FBG_4/FBG_1 in terms of Bragg wavelength shift permits to establish the position of an external concentrate force inducing mechanical deformation. Additionally the ratio of FBG_5/FBG_1 (in absolute value) is not dependent on mass and position along the panel length. As expected the ratio between compressive and tensile strain on opposite surfaces of a beam is dependent only on the beam structure/composition and not on the external forces. Moreover, it is worth noting the simultaneous measurement of FBG_5 and FBG_1 permits to estimate the position of the neutral axis, as schematically plotted in Fig. 5(d). In the miniaturized panel the neutral axis is found to be about $d_1 = 5.7\ \mu$m far from the FR4 surface and $d - d_1 = 3.3\ \mu$m from the copper film.

3.3 Deflection Calculation

In this section we report on the calculation of the miniaturized panel displacement along x axis by means of the approach presented in Section II when the panel is subjected to concentrated load as in previous section. According to the eq. (3), to meet this aim the strain profile along x axis has to be known.

It is worth noting that, in the present experimentation only two strain measurements points (FBG_1 and FBG_4) are available along x axis. However the deflection of a 1D solid beam due to a concentrated load in any position along x axis can be expressed by a third degree polynomial function [19] and thus the strain (and the angular moment) will be a linear function versus x axis. Accordingly, we can estimate the strain profile on the top layer surface taking into account only the strain measurement of FBG_1 and FBG_4 as we consider appropriate boundary condition in terms of zero strain at both panel ends ($x = 0$ and $x = 400$ mm). Fig. 6(a) plots the strain profile when the concentrate load is applied in position F_1 and F_2 with W_4 and W_3 weights. As expected, the maximum strain is in loading point and it decreases as the weight decreases and/or load moves away from the beam center.

Consequently, we can calculate the panel deflection by applying the eq. (3) as plotted in Fig. 6(b), taking into consideration the neutral axis position calculated in previous section. The constant C_1 and C_0 (due to double integration operation of the strain profile) are obtained by appropriate boundary condition. In particular the main boundary conditions are the continuity of deflection $\omega(x)$ and its first derivate $d\omega(x)/dx$ in the loading point ($x = F_1$ and $x = F_2$ for both cases). C_0 can be easily obtained by imposing zero deflection of the beam ends, even though the C_0 value is not important for our goal since it acts as an offset of the panel while it doesn't have effect on the deflection shape.

Fig. 6(b) shows the computed deflections when the concentrate load is applied in position F_1 and F_2 with W_4 and W_3 weights. As expected, the maximum deflection increases with load and the maximum deflection point moves from the panel center when the load is applied in position F_2. Finally, in order to validate the proposed approach, the case W_4 load in position F_1 is also compared with measurements of a mechanical comparator (with resolution of $+/-20\ \mu$m). The data exhibit a very good agreement. Maximum deflection of 178 μm was estimated by FBGs whereas the mechanical comparator provided a maximum deflection of 185 μm.

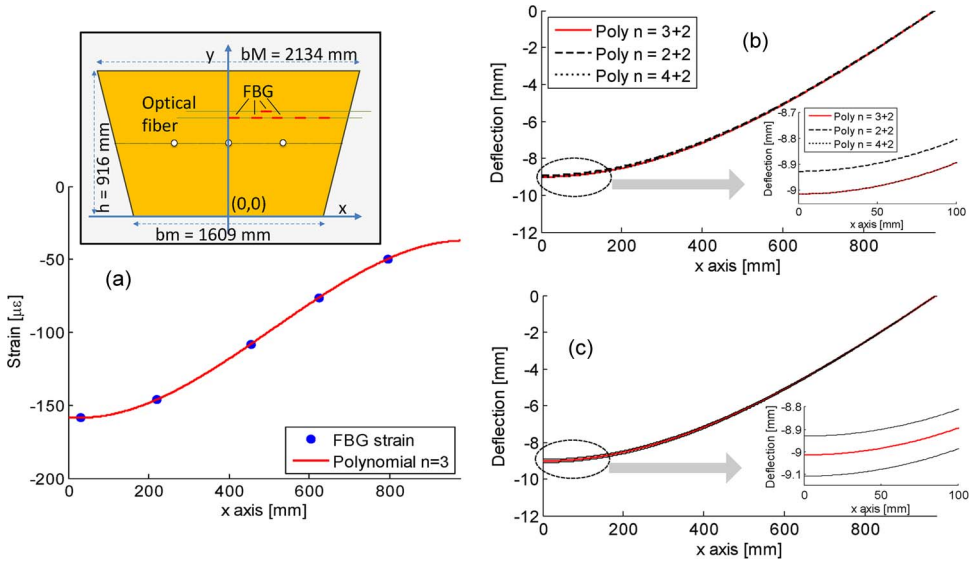

Fig. 7. (a) FBG strain measurements and 3 degree fitting. (Insert) Schematic top view of the full size panel; (b) calculated deflection as function of the strain fitting polynomial degree; and (c) and (b) deflection changes due to strain measurements error within $+/-2.0$ $\mu\varepsilon$.

4. Full Size Panel: Preliminary Results

In this section we present preliminary results of the deflection monitoring of the first full size drift panel of MM detector. The panel was realized at INFN laboratory in Pavia (Italy). The structure of the panel is similar to the miniaturized panel except for sizes: it exhibits a trapezoidal shape with height of h $=$ 916 mm, major base bM $=$ 2134 mm, minor base bm $=$ 1609 mm and thickness d $=$ 11.6 mm (including first FR4 layer of 500 μm, aluminium honeycomb core of 10.00 mm, second FR4 layer with copper film of 500 μm $+$ 35 nm and some layers of Araldite 1100 adhesive). A schematic of the top view of the panel is plotted in the insert of Fig. 7(a). Moreover, in order to increase its robustness the panel includes metal bars (about 30 mm large) along its edges and along horizontal and vertical center (for x $=$ 0 and y $=$ 458 mm).

Here, an FBG array including 5 polyamide coated sensors was bonded to the FR4 side along x axis for y $=$ 600 mm and x $= 3, 22, 45, 62, 80$ mm by means of Araldite adhesive. Two more gratings (FBG_6 and FBG_7) are bonded to the FR4 and copper side, respectively, in same position x $=$ 25 mm and y $=$ 630 mm. All FBG sensors were bonded to the panel when it was fixed on a high precision marble table ensuring perfectly planar state. To demonstrate the proposed approach in terms of deflection measurement the panel was then lift from the marble table by means of two metal bars 15 mm in height along the lateral sides. Consequently the panel deflects as consequence of its gravity load.

Fig. 7(a) shows the FBG measured strain state along the x axis (and y $=$ 600 mm) and its polynomial fitting with n $=$ 3 degree whereas the FBG_6 and FBG_7 responses permit to calculate the neutral axis position at about $d_1 = 6.2$ μm from the FR4 side and $d - d_1 = 5.4$ μm from the copper film. Fig. 7(b) plots the deflection of the panel computed by the eq. (3) and following boundary conditions: i) the maximum deflection is in the panel center $(x = 0)$ due to panel symmetry; and ii) zero deflection on the lateral edge. Here maximum deflection of 9.01 mm was achieved in perfect agreement with measurement provided by mechanical comparator.

The effect of the degree of the polynomial fitting was also evaluated. Fig. 7(b) plots the deflection profile achieved when the FBGs data were fitted with polynomial with n $=$ 2 and 4 too. As evident in the insert of Fig. 7(b) difference in maxim deflection calculation of 87 μm was found in between n $=$ 2 and n $=$ 3 fitting where no difference was found in between n $=$ 3 and n $=$ 4. This means that with 5 FBGs along the x axis for the detection of the strain profile the effect of the fitting degree is negligible. Deep studies about this issue involving FEM analysis are

currently in progress in order to find the best sensors number taking into consideration the desired requirements.

Finally, here also the effect of the finite resolution in FBG strain measurement was investigated. Even if our optoelectronic setup combined with centroid analysis for the Bragg wavelength identification can guarantee strain resolution less than $+/-0.5\ \mu\varepsilon$ a worst case was taken into consideration. Here independent random noise within $+/-2\ \mu\varepsilon$ was added to the 5 FBG measurements and the deflection was recalculated. By repeating 1000 times such procedure maximum and minimum deflection calculation versus x axis were plotted in Fig. 7(c). The insert reveal maximum error less than 190 μm while it decreases to 44 μm as we consider a strain resolution of $+/-0.5\ \mu\varepsilon$. These results ensure that resolution/error in the deflection evaluation due to the finite resolution in Bragg wavelength identification can meet the specification of the final tracking particle detector. It is worth noting that most of the commercial FBG interrogators guarantee wavelength resolution lower than 1 pm by appropriate centroid and/or fitting analysis of spectral shape.

5. Conclusion

In this paper we present a preliminary analysis on the use of FBG sensors integrated with tracking particle detector support panel as real-time deflection monitoring system. The results prove that the proposed approach has the potentialities to permit a continue monitoring of the deformation and bending of the support panels that currently are in phase of realization, testing and optimization. Further works will be addressed to implement the 2D analysis of the support panel. To this purpose numerical mechanical-analysis of the final detector will be used to reveal the number and optimized position of the FBG sensors to determinate all possible stretching and bending of the detector due to mechanical stress and undesired thermal change. Also, experimental testing aimed to investigate the possibility to use embedded FBG are currently in progress with very encouraging preliminary results. The achieved results of the proposed methodology let us believe that it will be take into consideration for the final update of ATLAS experiment.

Acknowledgement

We would like to thank all persons from University of Pavia and INFN “Sezione di Pavia” (Italy) for giving us the opportunity to test the FBG strain sensors on the first prototype of the MM drift panel. In particular, we would like to thank A. Giroletti, M. Grossi, A. Freddi, S. G. Gigli, C. Scagliotti, and F. Vercellati. Additionally we would like to thank INFN Roma1 for the miniature panel.

References

[1] “The CERN large Hadron Collider: Accelerator and experiments,” JINST 3, 2008.
[2] Y. Giomataris, P. Rebourgeard, J. Robert, and G. Charpak, “MICROMEGAS: A high granularity position sensitive gaseous detector for high particle flux environments,” *Nucl. Instrum. Methods Phys. Res. Section A, Accelerators, Spectrometers, Detectors Assoc. Equip.*, vol. A376, no. 1, pp. 29–35, Jun. 1996.
[3] ATLAS Collaboration, G. Aad *et al.*, “The ATLAS Experiment at the CERN Large Hadron Collider,” *J. Instrum.*, vol. 3, pp. S08003, Aug. 2008.
[4] T. Kawamoto *et al.*, “New small wheel technical design report,” CERN, Geneva, Switzerland, CERN-LHCC-2013-006, 2013.
[5] D. A. Krohn, *Fiber Optic Sensors: Fundamentals and Applications*. Durham, NC, USA: Instrumen. Syst. Autom. Soc., 2000.
[6] B. Culshaw, “Fiber optics in sensing and measurement,” *IEEE J. Sel. Topics Quantum Electron.*, vol. 6, no. 6, pp. 1014–1021, Nov./Dec. 2000.
[7] D. Sporea *et al.*, “Evaluation of UV optical fibers behavior under neutron irradiation,” *Adv. Mater. Phys. Chem.*, vol. 2, no. 4B, pp. 115–118, Dec. 2012.
[8] G. Rego *et al.*, “Effect of ionizing radiation on the properties of arc-induced long-period fiber gratings,” *App. Opt.*, vol. 44, no. 29, pp. 6258–6263, Oct. 10, 2005.
[9] G. Berruti *et al.*, “Radiation hard humidity sensors for high energy physics applications using polyimide-coated fiber Bragg gratings sensors,” *Sensors Actuators B*, vol. 177, pp. 94–102, Feb. 2013

[10] K. O. Hill and G. Meltz, "Fiber Bragg grating technology fundamentals and overview," *J. Lightw. Technol.*, vol. 15, no. 8, pp. 1263–222, Aug. 1997.
[11] A. Iadicicco, A. Cutolo, and A. Cusano, "Fiber Bragg grating sensors—Advancements and industrial applications," *Adv. Sci. Technol.*, vol. 55, pp. 213–222, 2008.
[12] A. Cusano, A. Iadicicco, D. Paladino, S. Campopiano, and A. Cutolo, "Photonic band-gap engineering in UV fiber gratings by the arc discharge technique," *Opt. Exp.*, vol. 16, no. 20, pp. 15 332–15 342, Sep. 2008.
[13] B. H. Lee, Y. Liu, S. B. Lee, S. S. Choi, and J. N. Jang, "Displacements of the resonant peaks of a long-period fiber grating induced by a change of ambient refractive index," *Opt. Lett.*, vol. 22, no. 23, pp. 1769–1771, Dec. 1997.
[14] F. Prudenzano *et al.*, "Optimization of pump absorption in MOF lasers via multi-long-period gratings: Design strategies," *Appl. Opt.*, vol. 51, no. 9, pp. 1410–1420, Mar. 2012.
[15] P. Steivurzel, E. D. Moore, E. C. Mägi, B. T. Kuhlmey, and B. J. Eggleton, "Long period grating resonances in photonic bandgap fiber," *Opt. Exp.*, vol. 14, no. 9, pp. 3007–3014, Apr. 2006.
[16] A. Iadicicco, S. Campopiano, and A. Cusano, "Long period gratings in hollow core fibers by pressure assisted arc discharge technique," *Photon. Technol. Lett.*, vol. 23, no. 21, pp. 1567–1569, Nov. 2011.
[17] A. Iadicicco, M. Della Pietra, and S. Campopiano, "FBG sensors for deformation monitoring of a tracking particle detector: Preliminary results," *Proc. SPIE*, vol. 9157, 91579L, 2014.
[18] A. Iadicicco, M. Della Pietra, and S. Campopiano, "Fiber Bragg grating strain sensors for tracking particle detector" *Proc. IEEE 3rd Mediterranean Photon. Conf.*, Trani, Italy, 2014.
[19] E. Carrera, G. Giunta, and M. Petrolo, *Beam Structures: Classical and Advanced Theories*. Hoboken, NJ, USA: Wiley, 2011
[20] S.-W. Kim, W.-R. Kang, M.-S. Jeong, I. Lee, and I.-B. Kwon, "Deflection estimation of a wind turbine blade using FBG sensors embedded n the blade bonding line," *Smart Mater. Struct.*, vol. 22, no. 12, pp. 125004-1–125004-11, Dec. 2013.